Data in brief 24 (2019) 103951

Contents lists available at ScienceDirect

Data in brief

journal homepage: www.elsevier.com/locate/dib

Data Article

Geochemical and mineralogical datasets on waters and stream precipitates from an abandoned mining site: Montevecchio-Ingurtosu district, Rio Irvi (SW Sardinia)

Nicola Rigonat*, Francesca Podda, Giovanni De Giudici, Daniela Medas

Dipartimento di Scienze Chimiche e Geologiche, Università degli Studi di Cagliari, Cittadella Universitaria di Monserrato, Blocco A, S.S. 554 bivio per Sestu, 09042, Monserrato (CA), Italy

A R T I C L E I N F O

Article history:
Available online 24 April 2019

A B S T R A C T

Geochemical modelling data and Powder X-Ray Diffraction data on samples collected along Rio Irvi (Montevecchio-Ingurtosu mining district, SW Sardinia, Italy) are reported in this paper. The data show the results of data processing to calculate water chemical speciation of ions and saturation indices of relevant mineral phases. These data are related with the research article: De Giudici G. et al (2018), Application of hydrologic-tracer techniques to the Casargiu adit and Rio Irvi (SW-Sardinia, Italy): Using enhanced natural attenuation to reduce extreme metal loads, Applied Geochemistry, vol.96, 42–54. The comparison of the calculated saturation indices of relevant Fe-bearing phases with the PXRD data of samples collected along the stream confirm the quality of the SI dataset and the good correlation between the calculations and the observed data.

The comparison of this dataset with others can help to deeper understand and quantify the impact of past and current mining activity on water bodies, contributing to implement the scientific background for the application of remediation actions.

* Corresponding author.
E-mail addresses: Nicola.rigonat@unica.it (N. Rigonat), fpodda@unica.it (F. Podda), gbgiudic@unica.it (G. De Giudici), dmedas@unica.it (D. Medas).

https://doi.org/10.1016/j.dib.2019.103951

Specifications table

Subject area	*Geology*
More specific subject area	*Environmental Mineralogy, Geochemistry*
Type of data	*Text file, tables, figures*
How data was acquired	*ICP-OES Fisons ARL 3520* *ICP-MS V Perkin Elmer SCIEX Elan DRC-e* *PXRD Panalytical Xpert Pro*
Data format	*Raw, filtered, analyzed*
Experimental factors	*30 synoptic stream water samples and 4 PXRD traces of stream precipitates*
Experimental features	*Samples analyzed in laboratory and geochemical data processed using PHREEQC and PXRD data using XPert High Score Plus.*
Data source location	*Rio Irvi, Casargiu, Montevecchio-Ingurtosu Mining District, Arbus municipality (Medio Campidano Province, SW Sardinia, Italy)*
Data accessibility	*Data are submitted with the paper*
Related research article	• De Giudici G., Medas D., Cidu R., Lattanzi P., Podda F., Frau F., Rigonat N., Pusceddu C., Da Pelo S., Onnis P., Marras P., Wanty R., Kimball B., Application of hydrologic-tracer techniques to the Casargiu adit and Rio Irvi (SW-Sardinia, Italy): Using enhanced natural attenuation to reduce extreme metal loads (2018), Applied Geochemistry, vol.96, 42–54 https://doi.org/10.1016/j.apgeochem.2018.06.004

Value of the data

- These datasets on geochemistry of a mining-affected stream are valuable for the study of provenance of contaminants in the waters of the Mediterranean basin.
- Identification of stream precipitates can help understanding the processes responsible for contaminant loads attenuation in mining-affected streams.
- Comparison of saturation indices data from datasets all over the world with the data here presented can offer insights on the possible presence of important biominerals in other streams.
- These data can support and be used to implement targeted effective remediation strategies.

1. Data

In this paper, a geochemical modelling dataset on water samples collected along the mining-affected Rio Irvi (SW Sardinia) is presented. Rio Irvi is a stream located in the Montevecchio-Ingurtosu mining district and is affected by mine drainage from an old flooded mine adit (Casargiu adit); as a result, the stream has very high contaminant loads, although attenuation processes that lead to the attenuation of Fe and SO_4^{2-} loads [1] thanks to the precipitation of Fe oxyhydroxides and sulphate-bearing green rust [2]. Furthermore, PXRD data of newly-formed mineral phases collected along Rio Irvi stream are presented.

The dataset shows the calculated speciation data and saturation indices (S.I.) of minerals and was produced by processing of water chemistry data using PHREEQC software. The images show the PXRD traces of stream precipitates.

2. Experimental design, materials, and methods

2.1. Hydrologic tracing and geochemical modelling

During the hydrologic campaign [1] along Rio Irvi, 30 instream sites were selected for water sampling. For each site, 5 aliquots were collected. One 0.45-μm filtered, unacidified for anion

determination via ion chromatography, two 0.45-μm filtered, acidified with 1% v/v with high purity NHO_3 for metal analysis (one for ICP-OES analysis, one for ICP-MS analysis), one unfiltered, acidified with 1% v/v with high purity NHO_3 for total recoverable metal analysis and one unfiltered, unacidified sample was collected for alkalinity, which was determined in the laboratory by Gran titration. Chemical data were then used to run geochemical modelling using PHREEQC [3] that allowed the calculation of ion speciation and Saturation Indices (S.I.) of mineral phases. Considering the significant role of geo-bio interactions in ruling metal mobility in polluted environments [4], geochemical modelling by PHREEQC was carried out using the 'wateq4f.dat' database implemented with the solubility constants (at 25 °C) of geological and biological hydrozincite (Eq. (1)) [5], hemimorphite (Eq. (2)) [6] and three relevant Fe and SO_4 bearing phases: SO_4-bearing Green Rust (Eq. (3)) [7] schwertmannite (Eq. (4)) and two-lines ferrihydrite (Eq. (5)) [8].

$$Zn_5(CO_3)_2(OH)_6 + 6H^+ \rightleftharpoons 5Zn^{2+} + 2CO_3^{2-} + 6H_2O \quad \log K = 6.2\,(\text{geo})\ \log K = 9\,(\text{bio}) \qquad \text{(Eq. 1)}$$

$$Zn_4Si_2O_7(OH)_2 \cdot H_2O + 8H^+ \rightleftharpoons 4Zn^{2+} + 2H_4SiO_4 + 2H_2O \quad \log K = 21.8 \qquad \text{(Eq. 2)}$$

$$Fe^{II}_4Fe^{III}_2(OH)_{12}SO_4 \cdot 8H_2O \rightleftharpoons 4Fe^{2+} + 2Fe^{3+} + 12OH^- + SO_4^{2-} + 8H_2O \quad \log K = -134.4 \qquad \text{(Eq. 3)}$$

Table 1
Speciation in aqueous phase of Fe, Zn and S, expressed as logarithm of activity.

	Distance	Fe^{2+}	$FeSO_4$	$FeOH^{2+}$	$Fe(OH)_3$	Fe^{3+}	SO_4^{2-}	$ZnSO_4$	Zn^{2+}	$Zn(SO_4)^{2-}$
	(m)	log(a)	log(a)	log(a)	log(a)	log(a)	log(a)	log(a)	log(a)	log(a)
CAS11-2	0	1.01E-03	1.30E-03	2.67E-07	3.77E-06	7.74E-11	7.81E-03	4.90E-03	2.76E-03	3.21E-04
CAS11-3	47	9.20E-04	1.22E-03	6.66E-07	6.66E-05	7.20E-11	7.94E-03	5.22E-03	2.88E-03	3.47E-04
CAS11-4	104	8.94E-04	1.15E-03	5.26E-07	3.38E-05	7.07E-11	7.67E-03	4.95E-03	2.83E-03	3.17E-04
CAS11-5	187	8.20E-04	1.04E-03	5.23E-07	3.77E-05	6.59E-11	7.56E-03	4.93E-03	2.85E-03	3.10E-04
CAS11-6	254	8.04E-04	1.02E-03	5.50E-07	4.17E-05	6.69E-11	7.48E-03	4.94E-03	2.87E-03	3.06E-04
CAS11-7	359	7.95E-04	1.08E-03	4.85E-07	2.59E-05	6.91E-11	7.88E-03	5.13E-03	2.81E-03	3.33E-04
CAS11-8	435	8.23E-04	1.04E-03	5.32E-07	2.97E-05	7.36E-11	7.23E-03	4.84E-03	2.88E-03	2.87E-04
CAS11-9	518	7.19E-04	9.41E-04	5.65E-07	4.46E-05	6.54E-11	7.48E-03	4.83E-03	2.77E-03	2.96E-04
CAS11-10	632	8.18E-04	1.04E-03	3.78E-07	1.03E-05	7.43E-11	7.25E-03	4.87E-03	2.88E-03	2.89E-04
CAS11-12	708	8.45E-04	1.11E-03	3.95E-07	1.06E-05	7.81E-11	7.48E-03	5.22E-03	2.99E-03	3.19E-04
CAS11-13	860	7.78E-04	1.03E-03	2.89E-07	4.60E-06	7.35E-11	7.48E-03	5.12E-03	2.93E-03	3.12E-04
CAS11-14	1061	7.77E-04	1.00E-03	2.98E-07	4.58E-06	7.62E-11	7.19E-03	5.11E-03	3.02E-03	2.97E-04
CAS11-16	1233	7.61E-04	9.39E-04	2.70E-07	3.92E-06	7.19E-11	6.96E-03	4.98E-03	3.05E-03	2.82E-04
CAS11-17	1373	7.59E-04	1.00E-03	2.48E-07	3.12E-06	7.13E-11	7.47E-03	5.30E-03	3.03E-03	3.22E-04
CAS11-18	1496	7.55E-04	9.83E-04	2.94E-07	5.44E-06	6.98E-11	7.40E-03	5.26E-03	3.05E-03	3.18E-04
CAS11-19	1626	7.51E-04	9.55E-04	2.07E-07	2.04E-06	6.79E-11	7.29E-03	4.86E-03	2.87E-03	2.90E-04
CAS11-20	1837	7.34E-04	9.35E-04	2.40E-07	3.60E-06	6.45E-11	7.36E-03	4.72E-03	2.77E-03	2.86E-04
CAS11-21	2142	7.48E-04	8.91E-04	1.76E-07	1.45E-06	6.40E-11	6.94E-03	4.57E-03	2.85E-03	2.62E-04
CAS11-22	2386	7.50E-04	9.60E-04	1.07E-07	3.76E-07	6.10E-11	7.60E-03	4.88E-03	2.80E-03	3.08E-04
CAS11-23	2557	7.23E-04	9.42E-04	1.48E-07	1.11E-06	5.79E-11	7.77E-03	4.81E-03	2.71E-03	3.11E-04
CAS11-24	2762	7.24E-04	9.35E-04	9.55E-08	3.07E-07	5.73E-11	7.73E-03	4.79E-03	2.71E-03	3.09E-04
CAS11-25	2974	7.35E-04	8.82E-04	1.70E-07	1.72E-06	5.78E-11	7.20E-03	4.61E-03	2.81E-03	2.77E-04
CAS11-26	3155	7.24E-04	8.88E-04	1.35E-07	8.65E-07	5.73E-11	7.35E-03	4.70E-03	2.80E-03	2.88E-04
CAS11-27	3535	7.27E-04	8.59E-04	1.12E-07	5.45E-07	5.56E-11	7.16E-03	4.61E-03	2.83E-03	2.77E-04
CAS11-28	3886	7.29E-04	8.81E-04	5.26E-08	6.46E-08	5.27E-11	7.46E-03	4.74E-03	2.82E-03	2.98E-04
CAS11-29	4279	7.04E-04	8.34E-04	5.46E-08	6.65E-08	5.39E-11	7.17E-03	4.74E-03	2.91E-03	2.85E-04
CAS11-30	4674	7.19E-04	8.59E-04	3.52E-08	1.71E-08	5.50E-11	7.24E-03	4.58E-03	2.79E-03	2.78E-04
CAS11-31	4963	7.00E-04	8.03E-04	2.65E-08	8.97E-09	5.06E-11	7.08E-03	4.43E-03	2.78E-03	2.66E-04
CAS11-32	5473	7.03E-04	7.89E-04	2.17E-08	4.84E-09	5.08E-11	6.93E-03	4.34E-03	2.78E-03	2.54E-04
CAS11-33	5872	7.12E-04	8.34E-04	1.57E-08	1.63E-09	5.35E-11	7.14E-03	4.53E-03	2.80E-03	2.72E-04

$$FeO(OH)_{0.75}(SO_4)_{0.125} + 2.75H^+ \rightleftharpoons Fe^{3+} + 0.125SO_4^{2-} + 1.75H_2O \quad \log K = 1.2 \qquad \text{(Eq. 4)}$$

$$Fe(OH)_3 + 3H^+ \rightleftharpoons Fe^{3+} + 3H_2O \quad \log K = 3.7 \qquad \text{(Eq. 5)}$$

Several relevant efflorescent salts frequently found in mining environments were added to the 'wateq4f.dat' database: szomolnokite (Eq. (6) [9]), melanterite (Eq. (7) [9]), coquimbite (Eq. (8) [10]), goslarite (Eq. (9) [11]) and mikasaite (Eq. (10) [12]).

$$Fe^{II}(SO_4)\cdot 4H_2O \rightleftharpoons Fe^{2+} + SO_4^{2-} + 4H_2O \quad \log K = -0.91 \qquad \text{(Eq. 6)}$$

$$Fe^{II}(SO_4)\cdot 7H_2O \rightleftharpoons Fe^{2+} + SO_4^{2-} + 7H_2O \quad \log K = -2.209 \qquad \text{(Eq. 7)}$$

$$Fe_2^{III}(SO_4)_3\cdot 9H_2O \rightleftharpoons 2Fe^{3+} + 3SO_4^{2-} + 9H_2O \quad \log K = -3.58 \qquad \text{(Eq. 8)}$$

Table 2
Saturation indices of relevant Fe-bearing phases.

	Distance	Green Rust (II)	Schwertmannite	Ferrihydrite	Goethite
	(m)	$Fe_6(OH)_{12}(SO_4)$:$8H_2O$	$FeO(OH)_{0.75}(SO_4)_{0.125}$	$Fe(OH)_3$	α-FeOOH
CAS11-2	0	0.47	4.46	3.68	8.24
CAS11-3	47	5.42	5.58	4.91	9.48
CAS11-4	104	4.22	5.3	4.6	9.18
CAS11-5	187	4.37	5.32	4.63	9.22
CAS11-6	254	4.58	5.33	4.63	9.24
CAS11-7	359	3.86	5.1	4.38	9.02
CAS11-8	435	4.14	5.12	4.41	9.06
CAS11-9	518	4.77	5.26	4.56	9.23
CAS11-10	632	2.33	4.68	3.93	8.6
CAS11-12	708	2.45	4.68	3.92	8.6
CAS11-13	860	0.97	4.32	3.54	8.23
CAS11-14	1061	1.02	4.28	3.49	8.21
CAS11-16	1233	0.64	4.25	3.47	8.16
CAS11-17	1373	0.26	4.17	3.37	8.06
CAS11-18	1496	1.19	4.41	3.63	8.31
CAS11-19	1626	−0.57	4.04	3.23	7.9
CAS11-20	1837	0.35	4.29	3.51	8.16
CAS11-21	2142	−1.29	3.96	3.14	7.77
CAS11-22	2386	−3.69	3.47	2.61	7.21
CAS11-23	2557	−1.87	3.92	3.1	7.69
CAS11-24	2762	−4.12	3.42	2.56	7.13
CAS11-25	2974	−1.16	4.11	3.31	7.89
CAS11-26	3155	−2.35	3.83	3.01	7.58
CAS11-27	3535	−3.22	3.68	2.84	7.4
CAS11-28	3886	−7.02	2.88	1.98	6.5
CAS11-29	4279	−6.9	2.84	1.93	6.49
CAS11-30	4674	−9.25	2.3	1.34	5.9
CAS11-31	4963	−10.51	2.09	1.12	5.64
CAS11-32	5473	−11.59	1.85	0.85	5.37
CAS11-33	5872	−13.38	1.38	0.34	4.88

Table 3
Saturation Indices of relevant Zn-bearing phases. The asterisks indicate that for those phases the S.I. could not be calculated because the concentration of CO_3 was below the detectability limit.

	Distance	Hydrozincite (geo)	Hydrozincite (bio)	Hemimorphite	Smithsonite
	(m)	$Zn_5(OH)_6(CO_3)_2$	$Zn_5(OH)_6(CO_3)_2$	$Zn_4Si_2O_7(OH)_2{*}H_2O$	$Zn(CO)_3$
CAS11-2	0	0.86	−1.94	7.7	−0.16
CAS11-3	47	4	1.2	11.11	0.12
CAS11-4	104	3.1	0.3	10.13	−0.01
CAS11-5	187	3.12	0.32	10.43	−0.07
CAS11-6	254	2.98	0.18	10.32	−0.13
CAS11-7	359	2.05	−0.75	9.73	−0.31
CAS11-8	435	2.2	−0.6	9.73	−0.24
CAS11-9	518	2.28	−0.52	10.19	−0.38
CAS11-10	632	0.15	−2.65	8.43	−0.78
CAS11-12	708	0.2	−2.6	8.43	−0.75
CAS11-13	860	−1.22	−4.02	7.43	−1.08
CAS11-14	1061	−1.17	−3.97	7.21	−1.01
CAS11-16	1233	−0.94	−3.74	7.27	−0.91
CAS11-17	1373	−1.29	−4.09	7.06	−0.99
CAS11-18	1496	−0.76	−3.56	7.79	−1
CAS11-19	1626	−1.77	−4.57	6.66	−1.08
CAS11-20	1837	*	*	7.34	*
CAS11-21	2142	*	*	6.41	*
CAS11-22	2386	*	*	5.05	*
CAS11-23	2557	*	*	6.39	*
CAS11-24	2762	*	*	4.98	*
CAS11-25	2974	−1.4	−4.2	6.84	−1.06
CAS11-26	3155	*	*	6.08	*
CAS11-27	3535	*	*	5.73	*
CAS11-28	3886	*	*	3.51	*
CAS11-29	4279	*	*	3.41	*
CAS11-30	4674	*	*	1.76	*
CAS11-31	4963	*	*	1.32	*
CAS11-32	5473	*	*	0.54	*
CAS11-33	5872	*	*	−0.88	*

Table 4
Saturation Indices of relevant Sulphates (Gp = gypsum, Anh = anhydrite, K-jar = Jarosite-(K), Szm = szomolnokite, Mel = melanterite, Coq = coquimbite, Mik = mikasaite, Gos = goslarite).

	Distance	Gp	Anh	K-jar	Szm	Mel	Coq	Mik	Gos
	(m)	$CaSO_4$ $*2H_2O$	$CaSO_4$	$KFe_3(SO_4)_2(OH)_6$	$FeSO_4$ $*4H_2O$	$FeSO_4$ $*7H_2O$	$Fe_2(SO_4)_3$ $*9H_2O$	$Fe_2(SO_4)_3$	$ZnSO_4$ $*7H_2O$
CAS11-2	0	−0.19	−0.42	5.6	−4.2	−2.9	−22.97	−27.35	−2.71
CAS11-3	47	−0.17	−0.41	8.08	−4.23	−2.93	−23.01	−27.4	−2.68
CAS11-4	104	−0.2	−0.43	7.49	−4.26	−2.96	−23.07	−27.46	−2.71
CAS11-5	187	−0.19	−0.42	7.46	−4.3	−3	−23.15	−27.54	−2.71
CAS11-6	254	−0.19	−0.42	7.53	−4.31	−3.01	−23.15	−27.54	−2.71
CAS11-7	359	−0.16	−0.38	7.09	−4.3	−3	−23.06	−27.44	−2.7
CAS11-8	435	−0.2	−0.42	7.14	−4.32	−3.02	−23.11	−27.5	−2.72
CAS11-9	518	−0.17	−0.39	7.48	−4.36	−3.06	−23.17	−27.56	−2.73
CAS11-10	632	−0.16	−0.38	6.26	−4.32	−3.02	−23.1	−27.49	−2.72
CAS11-12	708	−0.21	−0.43	6.31	−4.29	−2.99	−23.02	−27.4	−2.69
CAS11-13	860	−0.22	−0.44	5.48	−4.33	−3.03	−23.07	−27.46	−2.7
CAS11-14	1061	−0.21	−0.42	5.49	−4.34	−3.05	−23.09	−27.48	−2.71
CAS11-16	1233	−0.17	−0.39	5.3	−4.37	−3.07	−23.18	−27.57	−2.72
CAS11-17	1373	−0.22	−0.44	5.11	−4.34	−3.04	−23.1	−27.48	−2.69
CAS11-18	1496	−0.21	−0.43	5.62	−4.34	−3.05	−23.13	−27.51	−2.69
CAS11-19	1626	−0.2	−0.43	4.76	−4.35	−3.06	−23.17	−27.56	−2.72
CAS11-20	1837	−0.2	−0.42	5.26	−4.36	−3.06	−23.2	−27.59	−2.73
CAS11-21	2142	−0.19	−0.41	4.45	−4.38	−3.08	−23.29	−27.67	−2.75

(*continued on next page*)

Table 4 (*continued*)

	Distance	Gp	Anh	K-jar	Szm	Mel	Coq	Mik	Gos
	(m)	$CaSO_4$ *$2H_2O$	$CaSO_4$	$KFe_3(SO_4)_2(OH)_6$	$FeSO_4$ *$4H_2O$	$FeSO_4$ *$7H_2O$	$Fe_2(SO_4)_3$ *$9H_2O$	$Fe_2(SO_4)_3$	$ZnSO_4$ *$7H_2O$
CAS11-22	2386	−0.18	−0.41	3.34	−4.34	−3.04	−23.21	−27.6	−2.72
CAS11-23	2557	−0.2	−0.43	4.31	−4.34	−3.04	−23.23	−27.61	−2.72
CAS11-24	2762	−0.19	−0.42	3.2	−4.34	−3.05	−23.24	−27.63	−2.72
CAS11-25	2974	−0.2	−0.43	4.64	−4.37	−3.07	−23.33	−27.71	−2.74
CAS11-26	3155	−0.23	−0.46	4.12	−4.37	−3.07	−23.31	−27.7	−2.73
CAS11-27	3535	−0.19	−0.43	3.69	−4.38	−3.08	−23.37	−27.76	−2.74
CAS11-28	3886	−0.19	−0.43	1.93	−4.36	−3.06	−23.36	−27.75	−2.72
CAS11-29	4279	−0.2	−0.44	1.87	−4.39	−3.09	−23.39	−27.78	−2.72
CAS11-30	4674	−0.2	−0.43	0.7	−4.38	−3.08	−23.37	−27.75	−2.74
CAS11-31	4963	−0.17	−0.4	0.12	−4.4	−3.1	−23.47	−27.85	−2.75
CAS11-32	5473	−0.18	−0.42	−0.42	−4.4	−3.11	−23.49	−27.88	−2.76
CAS11-33	5872	−0.18	−0.41	−1.37	−4.39	−3.09	−23.41	−27.79	−2.74

$$ZnSO_4 \cdot 7H_2O \rightleftharpoons Zn^{2+} + SO_4^{2-} + 7H_2O \quad \log K = -1.96 \tag{Eq. 9}$$

$$Fe_2^{III}(SO_4)_3 \rightleftharpoons 2Fe^{3+} + 3SO_4^{2-} \quad \log K = 0.81 \tag{Eq. 10}$$

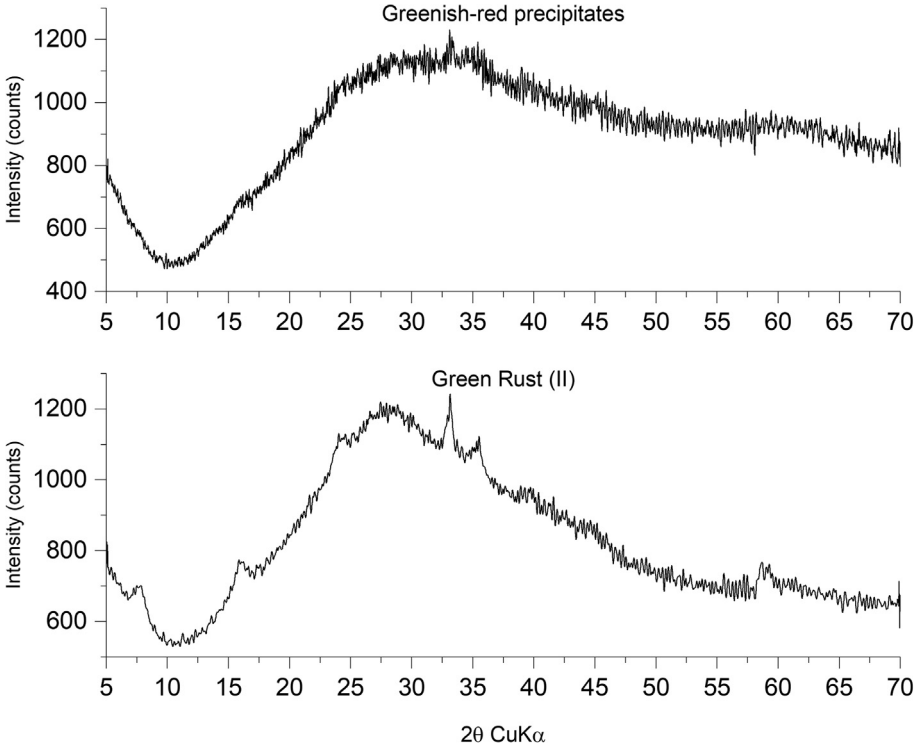

Fig. 1. PXRD traces amorphous greenish-red Fe oxyhydroxide and green flocculate (sulphate-bearing Green Rust, slightly oxidized into ferrihydrite).

Table 1 shows the ion speciation of Fe, Zn and S, Table 2 shows the Saturation indices of relevant Fe-bearing phases, Table 3 the Saturation Indices of relevant Zn-bearing phases and Table 4 the calculated saturation Indices of sulphates that are commonly found in mining-affected areas.

2.2. Sediment sampling and PXRD analysis

Four samples of sediments and flocculates were sampled along the river. The green colloidal green material (Green Rust II) was retained on a 0.45-μm paper filter upon water filtration and immediately frozen to prevent oxidation. The red material was collected from crusts covering the pebbles or from very fine muds filling stream pools.

After drying at room temperature, the red material was lightly ground in an agate mortar and subjected to Powder X-ray diffraction (PXRD) analysis, using conventional θ-θ equipment (PANalytical X'Pert Pro) with Cu Kα wavelength radiation (1.54060 Å), operating at 40 kV and 40 mA, using the X'Celerator detector (5–70°2θ window with 0.017°2θ step size). The resulting traces were processed using the X'Pert HighScore Plus (PANalytical B.V., Almelo, The Netherlands) to identify the mineral phases present. The green material was analysed directly on the filter paper to avoid oxidation. The PXRD traces (Fig. 1 and Fig. 2) were processed using X'Pert High Score Plus, with the following steps: $K\alpha_2$ stripping using the Rachinger method, trace smoothing using the Savitzky-Golay method (15 datapoints convolution range) and manual peak choice. The geochemical modelling based on the water samples collected along Rio Irvi presented in this study show a good correlation with the results of the mineralogical analysis of sediments sampled on the stream bed. These datasets will have significant importance for the development of a future environmental remediation plan for the Rio Irvi watershed and the understanding of the mineral precipitation processes along the stream.

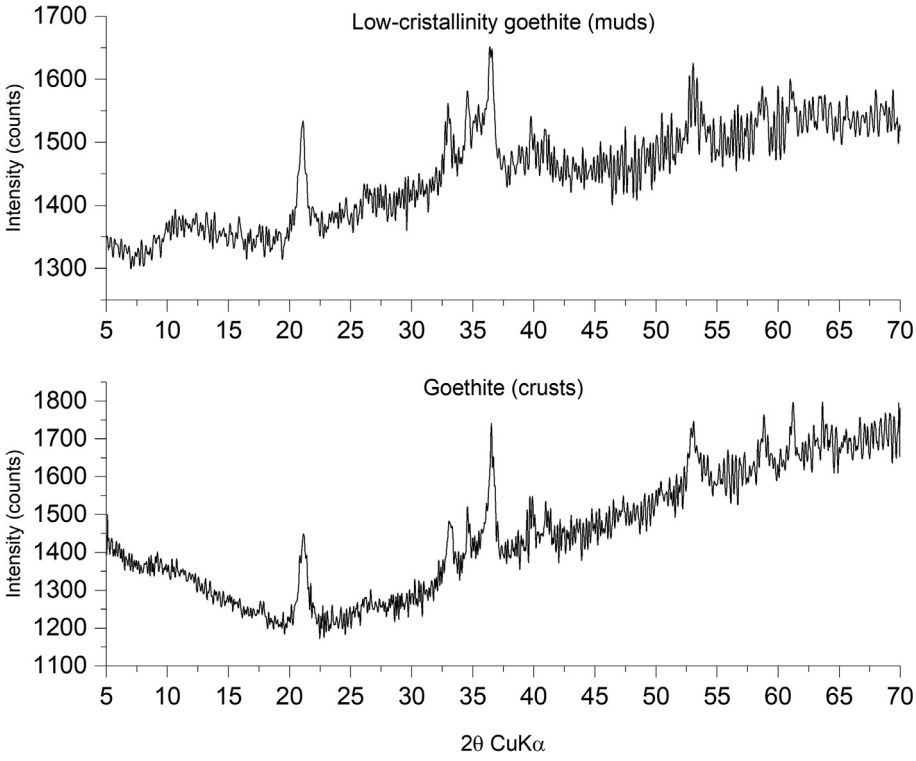

Fig. 2. PXRD traces of red precipitates, goethites with different crystallinity.

Acknowledgments

The authors acknowledge CESA (grant number: E58C16000080003) from RAS and RAS/FBS (grant number: F72F16003080002) grants, and FP7 ERANETMED2 72094 SUPREME.

The authors would like to thank R. Cidu, F. Frau, P.A. Marras, S. Da Pelo, R. Wanty and B.A. Kimball for their help and support during the hydrologic tracing campaign, the analysis of the samples and data processing.

Transparency document

Transparency document associated with this article can be found in the online version at https://doi.org/10.1016/j.dib.2019.103951.

References

[1] G. De Giudici, D. Medas, R. Cidu, P. Lattanzi, F. Podda, F. Frau, N. Rigonat, C. Pusceddu, S. Da Pelo, P. Onnis, P.A. Marras, R.B. Wanty, B. Kimball, Application of hydrologic-tracer techniques to the Casargiu adit and Rio Irvi (SW-Sardinia, Italy): using enhanced natural attenuation to reduce extreme metal loads, Appl. Geochem. 96 (2018) 42–54, https://doi.org/10.1016/j.apgeochem.2018.06.004.

[2] R. Cidu, F. Frau, Impact of the Casargiu mine drainage (sw Sardinia , Italy) on the mediterranean sea, in: Int. Mine Water Conf. 19th – 23rd Oct. 2009 Proc., 2009, pp. 926–931.

[3] B.D.L. Parkhurst, C. a J. Appelo, User's guide to PHREEQC (version 2) — a computer program for speciation, and inverse geochemical calculations, Exch. Organ. Behav. Teach. J. D (1999) 326. Repp. 99–4259.

[4] G. De Giudici, R.B. Wanty, F. Podda, B.A. Kimball, P.L. Verplanck, P. Lattanzi, R. Cidu, D. Medas, Quantifying biomineralization of zinc in the rio naracauli (Sardinia, Italy), using a tracer injection and synoptic sampling, Chem. Geol. 384 (2014) 110–119, https://doi.org/10.1016/j.chemgeo.2014.07.002.

[5] D. Medas, G. De Giudici, F. Podda, C. Meneghini, P. Lattanzi, Apparent energy of hydrated biomineral surface and apparent solubility constant: an investigation of hydrozincite, Geochem. Cosmochim. Acta 140 (2014) 349–364, https://doi.org/10.1016/j.gca.2014.05.019.

[6] R. Cidu, F. Frau, S. da Pelo, Drainage at abandoned mine sites: natural attenuation of contaminants in different seasons, Mine Water Environ. 30 (2011) 113–126, https://doi.org/10.1007/s10230-011-0146-4.

[7] F. Frau, D. Medas, S. Da Pelo, R.B. Wanty, R. Cidu, Environmental effects on the aquatic system and metal discharge to the mediterranean sea from a near-neutral zinc-ferrous sulfate mine drainage, Water, Air. Soil Pollut. 226 (2015), https://doi.org/10.1007/s11270-015-2339-0.

[8] J. Majzlan, A. Navrotsky, U. Schwertmann, Thermodynamics of iron oxides: Part III. Enthalpies of formation and stability of ferrihydrite (~Fe(OH)3), schwertmannite (~FeO(OH)3/4(SO4)1/8), and ε-Fe2O3, Geochem. Cosmochim. Acta 68 (2004) 1049–1059, https://doi.org/10.1016/S0016-7037(03)00371-5.

[9] E.J. Reardon, R.D. Beckie, Modelling chemical equilibria of acid mine-drainage: the FeSO4-H2SO4-H20 system, Geochem. Cosmochim. Acta 51 (1987) 2355–2368. https://ac.els-cdn.com/0016703787902900/1-s2.0-0016703787902900-main.pdf?_tid=c8016146-3adb-457b-9626-3ae08e1fea67&acdnat=1539091211_0ef54b5ae486a9cd5bce58a1cfead6d3. (Accessed 9 October 2018).

[10] P.L. Younger, S.A. Banwart, R.S. Hedin, Mine Water : Hydrology, Pollution, Remediation, Springer Netherlands, 2002. https://books.google.it/books?id=K7jxCAAAQBAJ&pg=PA96&lpg=PA96&dq=solubility+constant+coquimbite&source=bl&ots=upx_xHtk6M&sig=IH7LFZetAY16PoDxyh370jrdVVg&hl=en&sa=X&ved=2ahUKEwjJoMGSwvndAhVKxIUKHfZ4BeMQ6AEwE3oECAEQAQ#v=onepage&q=solubility constant coquimbite&f=false. (Accessed 9 October 2018).

[11] I. HydroGeoLogic, MINTEQA2/PRODEFA2, A Geochemical Assessment Model for Environmental Systems: User Manual Supplement for Version 4.0, 1998. Athens (Georgia), https://www.epa.gov/sites/production/files/documents/SUPPLE1.PDF. (Accessed 9 October 2018).

[12] S. Billon, P. Vieillard, Prediction of enthalpies of formation of hydrous sulfates, Am. Mineral. 100 (2015) 615–627, https://doi.org/10.2138/am-2015-4925.